TU Delft

Delft University of Technology

Fundamental Electromagnetic Configuration for Generating One-Directional Magnetic Field Gradients

Kosse, J.J.; Dhallé, M.; Rem, P.C.; ter Brake, H.J.M.; ten Kate, H.H.J.

DOI
10.1109/TMAG.2021.3080183

Publication date
2021

Document Version
Final published version

Published in
IEEE Transactions on Magnetics

Citation (APA)
Kosse, J. J., Dhallé, M., Rem, P. C., ter Brake, H. J. M., & ten Kate, H. H. J. (2021). Fundamental Electromagnetic Configuration for Generating One-Directional Magnetic Field Gradients. *IEEE Transactions on Magnetics*, *57*(8), Article 9430565. https://doi.org/10.1109/TMAG.2021.3080183

Important note
To cite this publication, please use the final published version (if applicable).
Please check the document version above.

Copyright
Other than for strictly personal use, it is not permitted to download, forward or distribute the text or part of it, without the consent of the author(s) and/or copyright holder(s), unless the work is under an open content license such as Creative Commons.

Takedown policy
Please contact us and provide details if you believe this document breaches copyrights.
We will remove access to the work immediately and investigate your claim.

This work is downloaded from Delft University of Technology.
For technical reasons the number of authors shown on this cover page is limited to a maximum of 10.

Fundamental Electromagnetic Configuration for Generating One-Directional Magnetic Field Gradients

J. J. Kosse[1], M. Dhallé[1], P. C. Rem[2], H. J. M. ter Brake[1], and H. H. J. ten Kate[1]

[1]Faculty of Science and Technology, University of Twente, 7522 NB Enschede, The Netherlands
[2]Faculty of Civil Engineering and Geosciences, Delft University of Technology, 2628 CD Delft, The Netherlands

In this article, electromagnet layouts are presented, which generate a magnetic field with a magnitude gradient that does not vary significantly in a horizontal plane but decreases monotonically with the vertical height above the magnet. Such a one-direction magnetic field gradient is a specific requirement for magnetic density separation (MDS), a novel recycling technology that combines a vertical magnetic field gradient with a ferrofluid to separate a mixture of non-magnetic materials based on their mass density. We are assembling the first superconducting magnet to be used for this application. In contrast to other separation technologies that use ferrofluid, multiple products can be separated in a single process step. First, the idealized current distribution is introduced that produces such a magnetic field with a magnitude that decays only in one direction. This ideal field can be approximated with practical coil configurations, which are evaluated with a Fourier analysis to derive an optimal cross-sectional layout based on flat racetrack coils. The analysis concludes with a discussion of the effect of winding pack thickness on the value of the magnetic field above the magnet system and the peak field inside the winding pack. The conclusions of this study are applicable not just for MDS but for any application that requires a magnetic field gradient that changes only in one direction.

Index Terms— **Ferrofluid, Fourier, harmonics, magnet, magnetic density separation (MDS), racetrack, vertical magnetic field gradient.**

I. Introduction

AT THE University of Twente, a superconducting NbTi demonstrator magnet for magnetic density separation (MDS) is under construction. MDS is a relatively new recycling technology that allows to separate a mixture of non-magnetic materials based on their mass density [1]–[6] and that ideally requires a magnetic field with a magnitude that only changes in the vertical direction.

The separation or filtration of magnetic materials with the aid of high-gradient magnetic fields is, of course, a well-established and widely used technology [7], [8] that was developed in the 1970s and 1980s [9], [10]. It essentially exploits the attraction of ferromagnetic, ferrimagnetic, or paramagnetic particles in the direction of the magnetic field gradient and is used in the purification of, e.g., coal [11]–[13], ores [14]–[16], and wastewater [17]–[20] or in the manipulation of various organic and biological materials [21]–[23]. Another widely used magnetic separation technique is eddy-current repulsion, typically used to extract non-ferrous metals out of waste streams [24], [25].

However, the separation of non-magnetic particles is enabled by the use of a ferrofluid in combination with a high-gradient magnetic field [26], where the magnetic force on the fluid competes with gravity (or centrifugal forces) to separate materials based on their specific density [8]. Before MDS, this method was limited to a binary sink-float approach. A major advantage of the MDS technology compared to these other types of magnetic separation is its ability to separate multiple components in a one-step process.

All these methods require a strong magnetic field gradient. What distinguishes MDS is that this gradient does not just need to be strong but ideally also one-directional. As discussed in Section II, variation of the magnetic field in a horizontal plane tends to re-mix the feed stream and hence needs to be minimized. This requirement is unique to MDS and leads to a specific design of the electromagnet, which is the main topic of this publication.

In the MDS process, shown in Fig. 1, shredded feed particles are immersed in a superparamagnetic fluid (ferrofluid) that flows over a magnet. The fluid is a colloid of superparamagnetic nanoparticles (usually water-based) [27], which is magnetically saturated using a magnet that generates a vertical magnetic field gradient [1]. The competition between gravity—acting on the feed particles—and magnetic attraction—acting on the ferrofluid—leads to a net force on the feed material that pushes it up, to an equilibrium height z_{eq}, which depends on its mass density. Different-density particles thus float at different heights in the fluid bed. A fluid flow drags the mixed feed stream from its insertion point toward separator blades that collect the different-density constituent materials. The ferrofluid is then recovered and the separated feed products go through further sensor sorting for final purification [6]. A transport belt moves over the magnet at the same speed as the fluid to reduce turbulence and to carry away any magnetic materials that may be present in the feed stream.

State-of-the-art MDS systems use permanent magnets (PMs), usually in the form of Halbach arrays [2], [29], [30], which imposes limits in terms of pole size and magnetic field strength. Superconductivity can enhance separation resolution

Manuscript received February 14, 2021; revised April 19, 2021; accepted May 3, 2021. Date of publication May 13, 2021; date of current version July 20, 2021. Corresponding author: J. J. Kosse (e-mail: j.j.kosse@utwente.nl).

Color versions of one or more figures in this article are available at https://doi.org/10.1109/TMAG.2021.3080183.

Digital Object Identifier 10.1109/TMAG.2021.3080183

This work is licensed under a Creative Commons Attribution-NonCommercial-NoDerivatives 4.0 License.
For more information, see https://creativecommons.org/licenses/by-nc-nd/4.0/

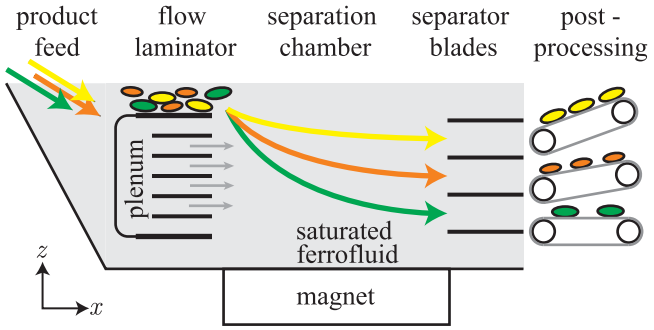

Fig. 1. Schematic of an MDS system. Feed material is shredded, wetted, and immersed into a ferrofluid flow. A magnet creates a vertical magnetic field gradient in the ferrofluid [2]. Particles move toward a height z that corresponds to their mass density. They can then be collected in different groups by separator blades.

while allowing for feeds of wider density ranges or more dilute ferrofluids, resulting in cost reduction. We are currently constructing a conduction-cooled NbTi-based MDS demonstrator for the separation of electronic material, e.g., shredded motherboards, that will constitute the first superconducting MDS system.

This magnet will consist of three NbTi/Cu racetrack coils with a width of 0.3 m each and a length of 1.4 m. The peak magnetic field in the coils is 5.2 T and the operating current 300 A. The magnet system will operate at 4.5 K, cooled by a closed-cycle cryocooler. The coils generate an average magnetic field of 2.0 T at the bottom of the fluid bed, with a vertical magnetic field gradient of magnitude 20 T/m [31]. The fluid bed is 0.9 m long in the flow direction, 1 m wide, and 0.3 m deep. Compared with the current PM-based MDS systems, which have a 0.6 T magnetic field at the fluid bed bottom and a pole size of 0.12 m [3], this design offers an increase in the separation resolution with a factor of 2.5. While superconducting systems have been developed for a variety of other separation systems [33]–[37], the required magnetic field profile is essentially different from that of MDS.

This article outlines how the electromagnetic design of the magnet relates to the desired field profile for this application. In Section II, the MDS operating principle is briefly presented, sketching how the forces on a feed particle are affected by the magnetic field profile and showing why the field magnitude ideally should change only with the vertical distance to the magnet, but not in a horizontal plane. The discussion also further clarifies how superconducting electromagnets may enhance this new technology.

In Section III, it is shown analytically how the generation of such an ideal field profile in principle requires an infinitely extended harmonic sheet current.

In Section IV and the Appendix, it is shown how such an ideal current distribution can best be approximated with a real magnet system. First, the Fourier analysis is used to optimize the 2-D current patterns that represent a system of flat racetrack-type magnets of varying complexity, and then, the thickness of the winding pack in a real 3-D implementation is considered, maximizing the magnitude of the useful field above the magnet and minimizing the peak field within the winding pack.

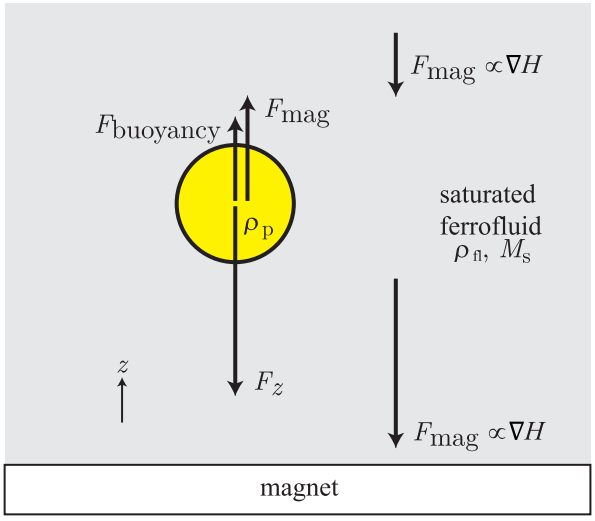

Fig. 2. Forces acting on a non-magnetic particle that is submerged in a magnetized ferrofluid in a vertical magnetic field gradient. The buoyant force and gravity are independent of height, whereas the magnetic force decays with increasing height.

II. MDS Operating Principle

Consider a particle with volume V and mass density ρ_{p}, submerged in a ferrofluid with density ρ_{fl} (see Fig. 2). In the absence of a magnetic field H, a particle denser than the ferrofluid will sink to the bottom of the fluid bed because the sum $\boldsymbol{F}_z + \boldsymbol{F}_{\text{buoyancy}}$ of the gravitational and buoyant forces is downward. When a magnet underneath the fluid is switched ON, the ferrofluid is attracted toward it. This causes an additional upward force $\boldsymbol{F}_{\text{mag}}$ on the non-magnetic particle.

This upward force is the opposite of the magnetic force that would act on the same volume of ferrofluid placed at the same location. It is given by [38]

$$\boldsymbol{F}_{\text{mag}} = -\nabla(\boldsymbol{m} \cdot \boldsymbol{B}) \tag{1}$$

with $\boldsymbol{m}$ the magnetic dipole moment of the displaced ferrofluid volume and $\boldsymbol{B}$ the local magnetic flux density. The ferrofluid is assumed to be magnetically saturated to a value M_{s} in the direction of the local magnetic field, so

$$\boldsymbol{m} \cdot \boldsymbol{B} = V M_{\text{s}} B(z). \tag{2}$$

With $\nabla M_{\text{s}} = 0$ and $\nabla B(z) = \mu_0 \nabla H(z)$, the magnetic force on the particle becomes

$$\boldsymbol{F}_{\text{mag}} = -\mu_0 M_{\text{s}} V \nabla H(z). \tag{3}$$

Note that this force is exerted on the non-magnetic particle by the surrounding fluid, not directly by the magnetic field. It can thus be regarded as a height-dependent buoyancy force.[1]

[1]The separation of materials with a density lower than that of the ferrofluid can be achieved by placing an (additional) magnet on top of the fluid bed [1].

At a certain equilibrium height z_{eq}, the net force on the particle in the vertical direction is zero [1], yielding

$$0 = F_z + F_{\mathrm{buoyancy}} + F_{\mathrm{mag}}(z = z_{\mathrm{eq}}) \tag{4a}$$

$$= (\rho_{\mathrm{fl}} - \rho_{\mathrm{p}})Vg - \mu_0 M_{\mathrm{s}} V \nabla_z H(z = z_{\mathrm{eq}}) \tag{4b}$$

where g is the gravitational acceleration. This expression can be simplified further by assuming a magnetic field with a magnitude that decays exponentially with height, with a characteristic decay length λ

$$H(z) = H_0 \exp\left(-\frac{2\pi}{\lambda} z\right). \tag{5}$$

The reasoning behind this choice is made clear in Section III. By inserting the (vertical) gradient of this magnetic field in the force balance [see (4b)], one obtains a closed expression for the equilibrium height

$$z_{\mathrm{eq}} = \frac{\lambda}{2\pi} \ln\left[\frac{2\pi \mu_0 M_{\mathrm{s}} H_0}{(\rho_{\mathrm{p}} - \rho_{\mathrm{fl}}) g \lambda}\right]. \tag{6}$$

For such an exponentially decaying field, z_{eq} does not depend on the horizontal coordinates (x, y) so that particles do not "wiggle" up and down as they are moving through the fluid bed. Also, as the magnetic force changes with the vertical coordinate, different-density particles will indeed float at different heights, which is the basis of the MDS process. In Section III, it is shown that an exponential field as in (5) is actually the only possible solution that meets these requirements perfectly.

The saturation magnetization M_{s} and the field strength H_0 appear in (6) as a product. This allows finding an optimal balance between capital expenditure and operational expenditure of an MDS installation. The first is dominated by the cost of the magnet system, and the second is dominated by the price of the ferrofluid [39]. Note that even though the fluid is recirculated, a fraction is lost during the cleaning of the sorted feed particles. Since superconducting magnets can generate stronger fields than PM systems, more dilute ferrofluids can be used. Also, a stronger field allows to lift—and thus to separate—heavier materials.

From (6), the vertical distance between the equilibrium heights of two different materials with densities ρ_1 and ρ_2 and the separation distance Δz can straightforwardly be derived as

$$\Delta z = z_{\mathrm{eq}}(\rho_2) - z_{\mathrm{eq}}(\rho_1) = \frac{\lambda}{2\pi} \ln\left(\frac{\rho_1 - \rho_{\mathrm{fl}}}{\rho_2 - \rho_{\mathrm{fl}}}\right). \tag{7}$$

This distance gives an indication of the obtainable separation resolution. As discussed in Section III, the decay length λ of the magnetic field strength scales with the size of the poles of the magnet, which is relatively limited for PM. Electromagnets in principle have no inherent size limitation since coils can be wound in arbitrary dimensions. A larger λ-value allows for an increased separation distance Δz for feed streams with a given density range $[\rho_1, \rho_2]$, enhancing the separation resolution compared to magnets with a more limited λ.

Section III considers the relation between the current distribution, i.e., the layout of an electromagnet, and the magnetic field profile in more detail.

III. Ideal Magnetic Field and the Required 2-D Current Distribution

In this section, it is shown how the optimal magnetic field for MDS is indeed described by (5). The vertical gradient of the magnetic field magnitude should not depend on the horizontal coordinates (x, y) so that the equilibrium height of the feed particles is constant in the horizontal plane. This minimizes particle "wiggling" and thus improves separation accuracy. We refer to such a magnetic field profile as the "ideal" field.[2] Mathematically, this requirement is expressed as

$$\frac{\partial^2 H}{\partial x \partial z} = 0, \quad \frac{\partial^2 H}{\partial y \partial z} = 0. \tag{8}$$

First, we consider the general case of a magnetic field above a unidirectional periodic sheet current with an arbitrary shape. From this, the sheet current distributions that satisfy (8) are identified, showing that only a pure harmonic sheet current generates such a field and that, hence, only an exponentially decaying field meets these requirements.

Consider a periodic sheet current $\boldsymbol{K} = K(x)\hat{\mathbf{y}}$ that flows at $z = 0$ in the y-direction in an infinite xy plane and is described as the Fourier series

$$K(x) = \sum_{n=0}^{\infty} K_n \cos\left(n\frac{2\pi}{\lambda}x + \phi_n\right). \tag{9}$$

We take every K_n to be positive. This can be achieved by multiplying any negative K_n by a factor -1 and adding a factor π to ϕ_n.

Above the current sheet, Ampére's law dictates that $\nabla \times \boldsymbol{H} = 0$ since, in this region, the current density is zero. This means that a scalar magnetic potential ψ can be invoked to solve the field

$$\boldsymbol{H} = \nabla \psi \tag{10}$$

by solving the Laplace equation

$$\nabla^2 \psi = 0. \tag{11}$$

A standard approach to solve (11) is by separation of variables, $\psi(x, z) = X(x)Z(z)$ [38]. The general solution to (10) and (11) can be written as

$$H_x = \sum_{n=0}^{\infty} \cos(k_n x + \theta_n)(a_n e^{+k_n z} + b_n e^{-k_n z}) \tag{12a}$$

$$H_z = \sum_{n=0}^{\infty} \sin(k_n x + \theta_n)(a_n e^{+k_n z} - b_n e^{-k_n z}). \tag{12b}$$

These equations are valid in general for any current-free region. The phases θ_n and the amplitudes a_n and b_n need to be derived from the boundary conditions, while k_n are separation constants.

[2]Horizontal field gradients are also of interest, as they can slow down, and even reverse, particle motion over the fluid bed. The main source of horizontal gradients is the truncation of the infinite xy plane to a finite-size magnet system, which is explored further in a separate paper [32].

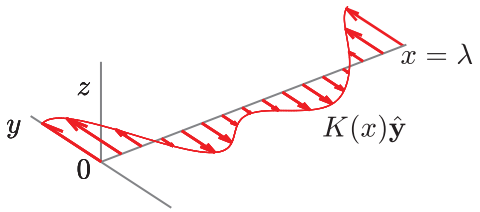

Fig. 3. Arbitrary sheet current $\boldsymbol{K}(x)$ with a magnitude that varies periodically with the horizontal coordinate x with period λ such that $\forall x$: $\boldsymbol{K}(x+\lambda) = \boldsymbol{K}(x)$.

Invoking once more Ampere's law, this time at the current sheet, the boundary condition at $z = 0$ can be expressed as

$$K(x) = \lim_{z\downarrow 0} H_x(x,z) - \lim_{z\uparrow 0} H_x(x,z) = 2\lim_{z\downarrow 0} H_x(x,z) \tag{13}$$

where the first limit represents the magnetic field just above the sheet and the second one just below. In combination with (9) and (12), (13) yields $k_n = 2\pi n/\lambda$; $\theta_n = \phi_n$ and $a_n + b_n = K_n/2$. Moreover, for a practical planar current distribution as in Fig. 3, currents need to return to the source so that the net current in the y-direction is zero and the trivial solution with $n = 0$ (corresponding to a uniform field generated by a uniform current sheet) may be excluded. In that case, the requirement that the field magnitude H remains finite for $z \uparrow \infty$ implies that all coefficients a_n must be zero, and the field generated by the periodic sheet current (9) becomes

$$H_x = +\sum_{n=1}^{\infty} \frac{K_n}{2} \cos\left(n\frac{2\pi}{\lambda}x + \phi_n\right) e^{-k_n z} \tag{14a}$$

$$H_z = -\sum_{n=1}^{\infty} \frac{K_n}{2} \sin\left(n\frac{2\pi}{\lambda}x + \phi_n\right) e^{-k_n z}. \tag{14b}$$

This is the general expression for the fields generated by periodic sheet currents of the type of (9). We can now verify which of these currents lead to a magnetic field that meets the requirement of (8), i.e. which currents lead to a one-directional field gradient. The magnitude of the field can be written as

$$H = \frac{1}{2}\left\{\sum_{n=1}^{\infty}\sum_{m=1}^{\infty} K_n K_m \cos\left[(n-m)\frac{2\pi}{\lambda}x + \phi_n - \phi_m\right] \times \exp\left[-(n+m)\frac{2\pi}{\lambda}z\right]\right\}^{0.5} \tag{15}$$

with partial derivate in the z-direction

$$\frac{\partial H}{\partial z} = \frac{1}{2H}\frac{\partial H^2}{\partial z} = -\frac{\pi}{4H}\sum_{n=1}^{\infty}\sum_{m=1}^{\infty}(n+m)K_n K_m \times \cos\left[(n-m)\frac{2\pi}{\lambda}x + \phi_n - \phi_m\right] \times \exp\left[-(n+m)\frac{2\pi}{\lambda}z\right]. \tag{16}$$

We require this function to be independent of x (see Criterion (8)). If n and m are equal, the cosine terms are independent of x and there are no restrictions on K_n. However, if n and m are unequal, this will not be the case. One must therefore make sure that these cross terms do not contribute.

For every contribution in the dual sum where n and m are unequal, the cosine term has to be extinguished by the coefficients that determine its amplitude. This cannot be done by the factor $(n + m)$, which is always positive. Thus, we need to place demands on the product of the coefficients K_n and K_m

$$\sum_{n=1}^{\infty}\sum_{\substack{m=1\\ m\neq n}}^{\infty} K_n K_m = 0. \tag{17}$$

This means that only a single term K_n can be non-zero. In other words, only a pure harmonic sheet current will produce a field with a purely one-directional magnitude gradient. In that case, one may as well set $K_1 \neq 0$, choose the phase angle ϕ_1 to be zero, and write

$$\boldsymbol{K} = K_1 \cos\left(\frac{2\pi}{\lambda}x\right)\hat{\mathbf{y}} \tag{18}$$

$$H_x = +\frac{K_1}{2}\cos\left(\frac{2\pi}{\lambda}x\right)\exp\left(-\frac{2\pi}{\lambda}z\right) \tag{19}$$

$$H_z = -\frac{K_1}{2}\sin\left(\frac{2\pi}{\lambda}x\right)\exp\left(-\frac{2\pi}{\lambda}z\right) \tag{20}$$

$$H = \frac{K_1}{2}\exp\left(-\frac{2\pi}{\lambda}z\right). \tag{21}$$

IV. Racetrack Coils: Optimization of the 2-D Current Distribution

Realizing a cosine-shaped sheet current distribution as described by (18) is not practical since it would require a complicated coil layout. In this section, more realistic current distributions are considered, which approximates such an ideal current distribution. The corresponding deviations from the ideal magnetic field [see (19)–(21)] can be expressed in terms of Fourier coefficients. First, in Section IV-A, the effects of moving from a continuous to a discrete 2-D current distribution are considered. This allows to model an infinite array of thin racetrack coil and thus to optimize the shape of the coils. Then, in Section IV-B, the effect of a finite winding pack thickness (in the z-direction, see Figs. 3 and 4) is included, switching from a 2-D sheet current to a 3-D volume current and exploring the consequences both for the useful field above the coils and for the peak field within the winding pack. Also, this analysis will still consider an infinite array of coils. End effects caused by truncating the periodic current distribution to a finite number of coils (in the x-direction) with a finite length (in the y-direction) are not considered in this article, but discussed elsewhere [32].

A. Optimal Discrete Racetrack Geometry

A magnet system that is practical to produce is a series of flat racetrack coils, as shown in Fig. 4. These are electromagnets that consist of two straight coil sections, each with a width w, which are connected by two semicircular "heads." Assuming that a homogeneous current distribution in the winding pack allows to model the magnetic field

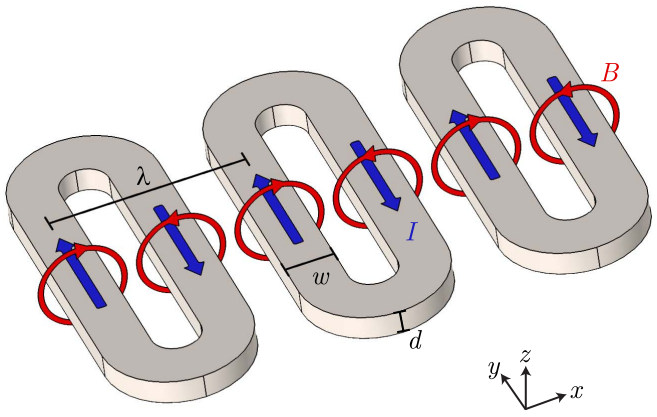

Fig. 4. Sketch of a magnet consisting of three flat racetrack coils. The current direction is shown by blue straight arrows, and the magnetic field direction is shown by red circular arrows. Coils are translated by a distance λ relative to each other in the x-direction.

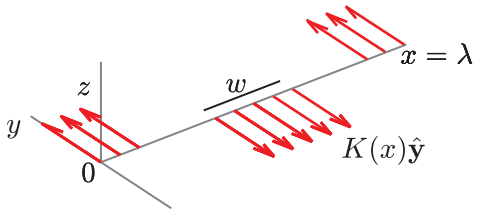

Fig. 5. Sheet current $\boldsymbol{K}(x)$ that has a magnitude varying stepwise with the horizontal coordinate x with period λ. This rectangular current distribution represents one period of the coil layout of the racetracks in Fig. 4.

produced by such a coil accurately, thus one does not need to consider the individual wires within the winding pack [40].[3] In the following analysis, we focus on the xz cross section corresponding to the y-symmetry plane.[4]

Consider an infinite number of such racetrack coils, translated a distance λ from each other in the x-direction. In this section, the relative thickness of the coils d/λ is still assumed to be small enough to approximate the volume current density $\boldsymbol{J}$ by a surface current density $\boldsymbol{K}(x) = \boldsymbol{J}(x)d$. The corresponding sheet current then consists of alternating regions, where $\boldsymbol{K}(x)$ is either $+K_0\hat{\mathbf{y}}$, zero, or $-K_0\hat{\mathbf{y}}$ with periodicity λ, as in Fig. 5. The question that can then be addressed is which racetrack leg width w yields the best approximation of the ideal field.

To determine an optimal value for w/λ, the discrete Fourier components of the sheet current are of interest. To answer this question, we develop this current distribution as a Fourier series, such as in (9). Choosing $x = 0$ in the center of one of the racetrack legs, we can exploit the symmetry $K(x) = K(-x)$ to set all the phases ϕ_n to zero

$$K(x) = \sum_{n=1}^{\infty} K_n \cos\left(n\frac{2\pi}{\lambda}x\right) \tag{22}$$

[3]On condition that a correct packing factor is considered.

[4]In an MDS system, the direction of the fluid flow could be either in the x- or y-direction.

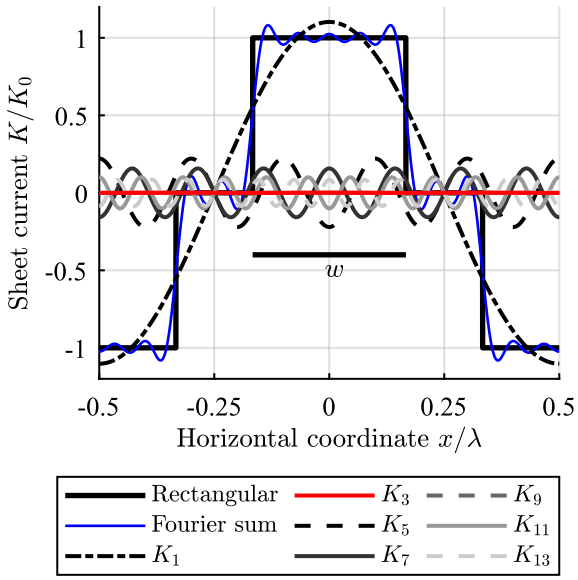

Fig. 6. Rectangular (black solid line) sheet current distribution with periodicity λ and width $w = \lambda/3$. The current distribution can be expanded into a Fourier series, in which terms (up to $n = 13$) are plotted. The sum of the terms is the blue thin solid line. The K_1 term (black dashed-dotted line) represents the ideal current distribution.

where, as discussed above, we omitted the $n = 0$ term to consider that the net current in the y-direction is zero.

For a current distribution as in Fig. 5, the Fourier coefficients K_n can straightforwardly be derived to be

$$K_n = \frac{2K_0}{n\pi}\sin\left(n\frac{w}{\lambda}\pi\right)[1-\cos(n\pi)] \tag{23}$$

where K_0 is a scaling term. It is set to 1 in the remainder of this article for simplicity. An example of such a Fourier expansion is shown in Fig. 6, and for the specific case, $w/\lambda = 1/3$. Note that the components with n even are zero. The field generated by this current distribution can then be derived from (14a) and (14b). As shown by (16), the presence of the higher harmonics $n = 3, 5, \ldots$ leads to an undesired x-component of ∇H. It is therefore important to minimize the influence of K_3 and higher components. However, compared with our desired $n = 1$ term, these higher harmonics decay fast with the height z above the magnet, due to the factor n in the exponent. In other words, at larger distances, lower order Fourier components contribute more to the magnetic field than the higher order ones. To approximate the ideal field as closely as possible, it is therefore especially important to minimize the lower order harmonics.

In Fig. 7, the first terms of the Fourier expansion are shown as a function of the current sheet width w/λ. By investigating (23), it can be seen that the nth component has zero magnitude whenever $w/\lambda = 1/n$. Thus, by setting the width of the current sheets equal to exactly one-third of the coil system periodicity, $w/\lambda = 1/3$, *the amplitude of the—principal unwanted—third harmonic can be made zero* (and, more general, all K_{3+6m} with m integer).

Note that this does not necessarily mean that a racetrack coil needs a leg width of $\lambda/3$. One can also use racetracks

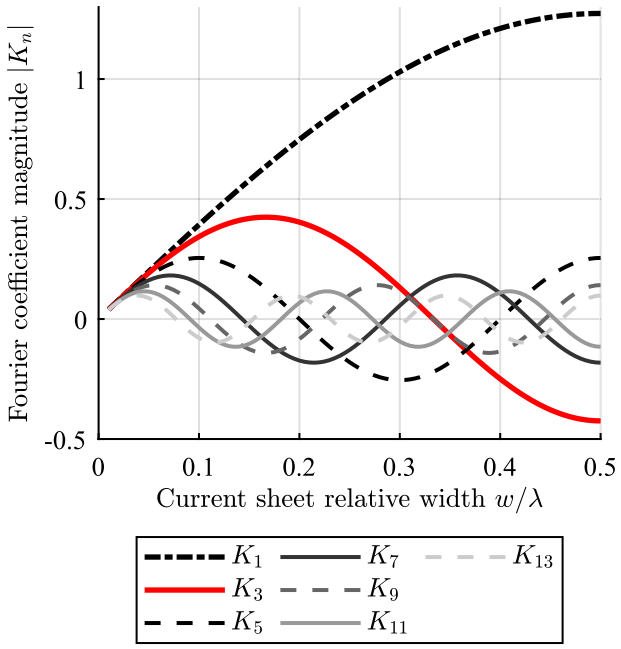

Fig. 7. Variation of the magnitude of the magnetic field Fourier components as a function of current sheet width. The nth component is zero at $w/\lambda = 1/n$.

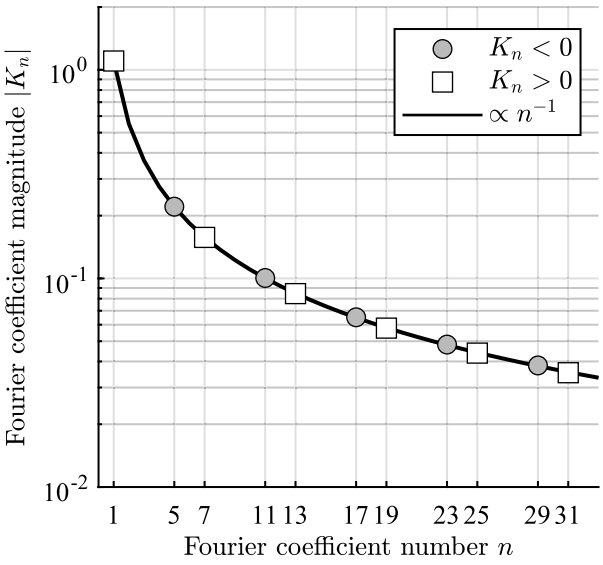

Fig. 8. Variation of the magnitude of non-zero Fourier components for the rectangular current distribution in Fig. 5, for a width $w/\lambda = 1/3$. Components are plotted up to $n = 31$. Square markers: positive values. Round markers: negative values.

with leg width $\lambda/6$ placed adjacent to each other, with the current flowing in the same direction for touching legs.

Plotting the magnitude of the remaining Fourier components for $w/\lambda = 1/3$ results in Fig. 8. With K_3 removed, K_5 is the largest remaining unwanted component. A practical way of eliminating this component is by adding five subdivisions of period $\lambda/5$ and amplitude $(2/5\pi)\sin((5/3)\pi)$ to the original current sheet profile. This type of current distribution may be called a notched distribution. However, eliminating K_5 (and possibly higher order Fourier coefficients) comes at the price of a more complex winding pack. More details on such further refinement of the current distribution can be found in the Appendix.

B. Effect of Winding Pack Thickness

A real coil has, of course, a finite winding pack thickness d and carries a volumetric current density instead of a sheet current. This has consequences not only for the magnetic field in the fluid bed, where generally the highest possible magnitude is desired, but also for the field experienced by the conductor from which the coil is wound. Note that in superconducting electro-magnets, the peak magnetic field on the windings limits their current-carrying properties and should therefore be kept as low as possible [41], [42].

For the magnetic field in the fluid bed, the effect of the winding pack thickness on the field magnitude is of interest, as well as—for the rectangular current distributions—the change in ripple, which as discussed above is represented by the higher order Fourier coefficients. Inside the winding pack, we will show how the effect on the peak magnetic field differs for the ideal current distribution and the rectangular current distribution.

We start once more by considering the ideal pure harmonic current configuration and work out the magnetic field magnitude at a height z above the conductor when we gradually increase the winding pack thickness d while keeping the current density J_0 in the winding pack constant.

This can be done by integrating the field contributions generated by a series of parallel sheet currents of infinitesimal thickness $\mathrm{d}z'$ located in the range $z' = [-d, 0]$, each carrying a current amplitude $K_1 = J_0\,\mathrm{d}z'$. Note that with this choice of coordinates, $z = 0$ corresponds to the top of the winding pack. Referring to (19) and (20), we can write

$$H_x = \frac{J_0}{2}\cos\left(\frac{2\pi}{\lambda}x\right)\int_{z'=-d}^{z'=0}\exp\left(-\frac{2\pi}{\lambda}(z-z')\right)\mathrm{d}z' \quad (24a)$$

$$= \frac{J_0\lambda}{4\pi}\cos\left(\frac{2\pi}{\lambda}x\right)\exp\left(-\frac{2\pi}{\lambda}z\right) \times\left[1-\exp\left(-\frac{2\pi}{\lambda}d\right)\right] \quad (24b)$$

and analogously

$$H_z = -\frac{J_0\lambda}{4\pi}\sin\left(\frac{2\pi}{\lambda}x\right)\exp\left(-\frac{2\pi}{\lambda}z\right) \times\left[1-\exp\left(-\frac{2\pi}{\lambda}d\right)\right] \quad (25)$$

$$H = -\frac{J_0\lambda}{4\pi}\exp\left(-\frac{2\pi}{\lambda}z\right)\left[1-\exp\left(-\frac{2\pi}{\lambda}d\right)\right]. \quad (26)$$

Note that in the limit $d \to 0$ the expression reduces to (21).

The value of the field magnitude just above the winding pack (at $z = 0$) is plotted against winding pack thickness in Fig. 9. For coils much thinner than $\lambda/2\pi$, the magnitude increases linearly with coil thickness, as may be expected, but for coils much thicker than $\lambda/2\pi$, additional windings added at the bottom are too far away to contribute significantly and the field magnitude saturates at $H = J_0\lambda/4\pi$.

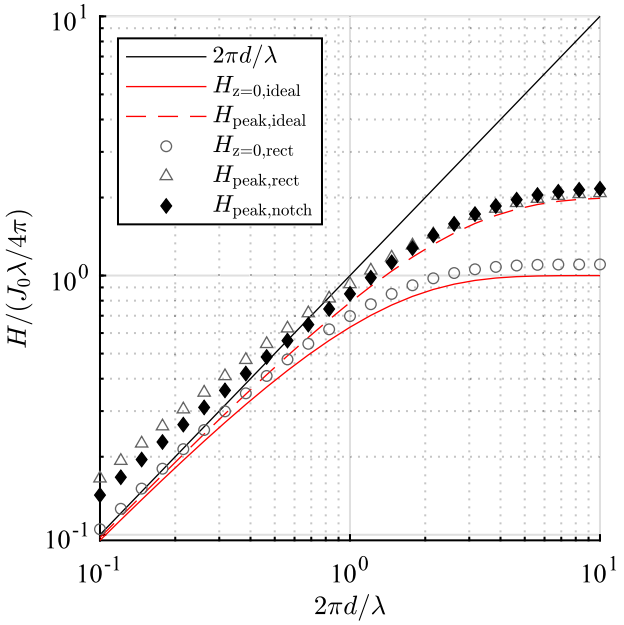

Fig. 9. Scaled magnetic field magnitude as a function of coil thickness. The red solid line indicates the field at the surface of the coils for an ideal harmonic current distribution, and the red dashed line indicates the peak magnetic field on the conductor. The round markers indicate the field at the surface of the coils for a rectangular current distribution, and the triangular markers indicate the peak magnetic field on the conductor.

The magnetic field components inside the current-carrying space ($-d \le z \le 0$) are

$$H_x = +\frac{J_0\lambda}{4\pi}\cos\left(\frac{2\pi}{\lambda}x\right) \times\left[\exp\left(\frac{2\pi}{\lambda}z\right) - \exp\left(-\frac{2\pi}{\lambda}(z+d)\right)\right] \tag{27}$$

$$H_z = -\frac{J_0\lambda}{4\pi}\sin\left(\frac{2\pi}{\lambda}x\right) \times\left[2 - \exp\left(\frac{2\pi}{\lambda}z\right) - \exp\left(-\frac{2\pi}{\lambda}(z+d)\right)\right]. \tag{28}$$

These expressions are obtained by summing two integrals: the first spanning $[-d, z]$ and the second $[z, 0]$. It can be proved that the maximum magnetic field is located at $z = -d/2$ by solving $\partial H^2/\partial x = 0$ and $\partial H^2/\partial z = 0$. The maximum magnetic field inside the current-carrying space is given by

$$H_{\text{peak}} = \frac{J_0\lambda}{2\pi}\left[1 - \exp\left(-\frac{\pi}{\lambda}d\right)\right]. \tag{29}$$

Also, (29) is plotted in Fig. 9. The rate of increase of the peak field with winding pack thickness decreases as the winding pack gets thicker but saturates at a higher thickness compared to the field on the surface.

The ratio of the effective magnetic field magnitude at the surface of the coils to the peak magnetic field on the conductor scales as

$$\frac{H_{z=0}}{H_{\text{peak}}} \propto \frac{1 - \exp\left(-\frac{2\pi}{\lambda}d\right)}{1 - \exp\left(-\frac{\pi}{\lambda}d\right)} = 1 + \exp\left(-\frac{\pi}{\lambda}d\right). \tag{30}$$

As the winding pack is made thicker, the relative increase of the peak magnetic field is larger than that of the magnetic field at the surface and this holds for all thicknesses d. Intuitively, one may expect that this result also holds for rectangular current distributions. However, analysis in detail of these distributions, for both the "simple" and notched versions, shows that this is not the case.

As a start, the mean magnitude of the magnetic field above the rectangular and notched configurations can be accurately approximated by (26) when including a small scaling term $K_1 \approx 1.10K_0$ (open circles in Fig. 9). The fact that K_1 is slightly larger than K_0 for $w = \lambda/3$ can also be seen in Fig. 6.

What is significantly different, however, is the relation between the peak magnetic field on the rectangular volume current distribution and the winding pack thickness. This peak field can be shown to be, once more using integration of the field components

$$H_{z=-d/2,\text{rect}} = \frac{J_0\lambda}{2\pi}\sum_{n=1}^{\infty} K_n \sin\left(n\frac{2\pi}{\lambda}x\right) \times\left[1 - \exp\left(-n\frac{\pi}{\lambda}d\right)\right]. \tag{31}$$

This function varies with x, and the maximum is of interest

$$H_{\text{peak,rect}} = \max_{-\lambda/2 \le x \le \lambda/2} [H_{z=-d/2,\text{rect}}(x)]. \tag{32}$$

This maximum as a function of coil thickness is shown in Fig. 9, for both a rectangular and notched configuration (both with $w/\lambda = 1/3$). For thin winding packs, a strong increase relative to the ideal current distribution is visible.

The higher order harmonics decay quickly with distance, so they do not influence the magnetic field significantly at the fluid bed, whereas they do affect the peak magnetic field in the winding pack. The thinner the coils are, the larger is the influence of the higher harmonics on the peak field. For a thicker winding pack, the harmonics are generated at a larger distance from the peak field location, and due to their rapid decay, their effect on the peak field is smaller.

By comparing the peak field of the notched configuration against the simple rectangular one, it can be observed that the effect of notching is the biggest for thin winding packs. For thin coils, the K_5 component and its multiples ($K_{10}, K_{15}, \ldots$) increase the peak field on the simple rectangular conductors, whereas for the notched configuration, these harmonics are zero. For larger winding pack thicknesses, these components have decayed relative to the K_1 component at the peak field location, and as such, the notching has less effect on the peak field magnitude.

Some counter-intuitive behavior due to the sharp increase of the peak magnetic field for thin coils can be seen when comparing the effective mean-field magnitude at the surface of the coils with the peak field in the conductor. The ratio of these functions is plotted in Fig. 10, for the rectangular (blue) and notched (gray) configurations. They show a maximum at a non-zero winding pack thickness. Thus, the intuitive result found for an ideal distribution does not hold; adding extra windings, i.e., making thicker coils, can provide a relative boost to the obtained gradient in the fluid larger than the accompanying increase in peak field in the conductor.

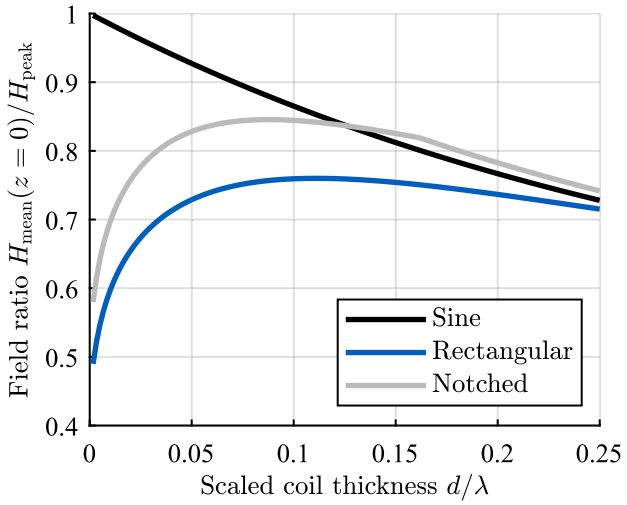

Fig. 10. Ratio between the average magnetic field at the surface of the coils ($z = 0$) and the peak field within the coils as a function of coil thickness.

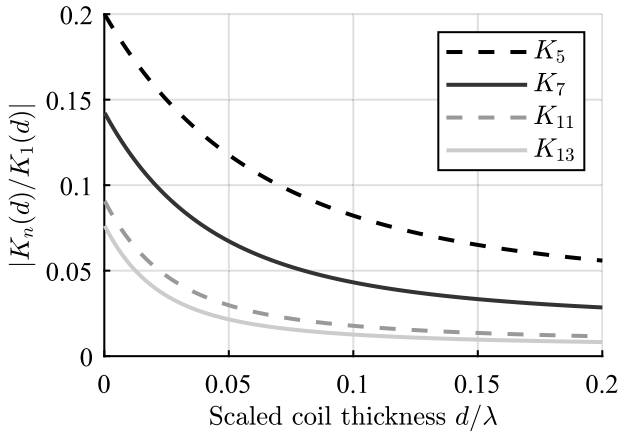

Fig. 11. Magnitude of the non-zero Fourier components (up to $n = 13$), plotted as a function of winding pack thickness, relative to the K_1 component at that thickness.

Next, the change in ripple of the magnetic field at the fluid bed as a result of the finite winding pack thickness is considered. As the magnetic field is ripple-free when generated by the "ideal" sheet current distribution [see (18)], it will also be ripple-free when generated by a sum of parallel ideal sheet currents (i.e., an ideal volume current distribution).

For racetrack coils, moving from a sheet current to a volume current shows a change in the amplitude of the Fourier coefficients at the top of the winding pack. Each sheet current Fourier component is considered to be effectively reduced in magnitude at the top of the winding pack by a factor $\exp(-n(2\pi/\lambda)z')$, where z' is the location of that current sheet

$$K_{n,\text{volume}}(z=0,d) \tag{33a}$$

$$= \frac{K_n}{d}\int_{z'=-d}^{z'=0} \exp\Big[-n\frac{2\pi}{\lambda}(-z')\Big]\,\mathrm{d}z' \tag{33b}$$

$$= \frac{K_n}{d}\frac{\lambda}{2\pi n}\Big[1-\exp\Big(-n\frac{2\pi}{\lambda}d\Big)\Big]. \tag{33c}$$

In Fig. 11, the effective magnitudes of the Fourier components are shown as a function of winding pack thickness, relative to the K_1 component at this particular thickness. At $d = \lambda/12$, the value coinciding with our demonstrator magnet design, the contribution of the K_5 component is more than halved compared to its value for a single current sheet.

Moving from a sheet current to a volume current thus has a positive effect on the ratio of the effective fluid bed magnetic field to peak magnetic field, as well as on reducing the magnetic field ripple at the fluid bed.

To visualize the influence of a thicker winding pack, Fig. 12 shows the magnetic field above a periodic array of racetrack coils with characteristic width $\lambda/3$ for three different winding pack thicknesses.

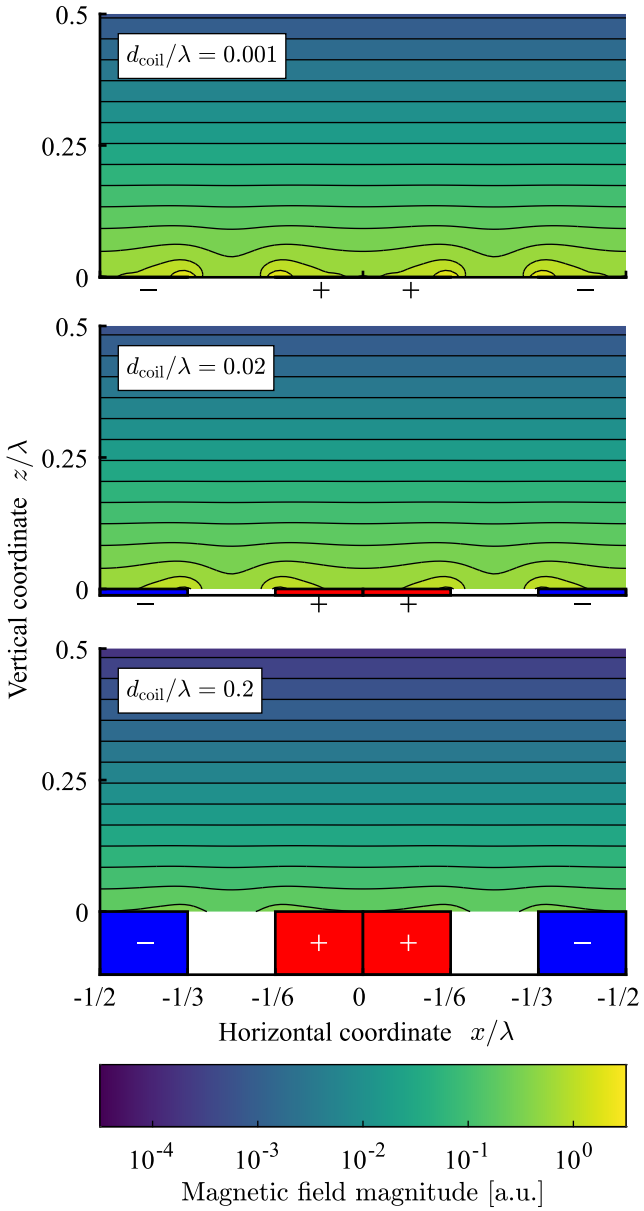

Fig. 12. Magnetic field magnitude above configurations consisting of an infinite number of racetrack coils, for varying thicknesses of the winding pack (scaled to the periodicity λ). Two coils are plotted (each with a width $\lambda/2$), and the polarity of the current is indicated by a red color with a plus sign and a blue color with a minus sign. Thicker coils produce a smoother field, as the K_1 component is relatively large compared to the higher order components.

The Fourier components of (33) are entered in (15) to obtain the expression for the magnetic field magnitude generated by a coil set with a non-zero winding pack thickness, valid for $z > 0$

$$H = \frac{1}{2}\left\{\sum_{n=1}^{\infty}\sum_{m=1}^{\infty}\left(\frac{\lambda}{2\pi d}\right)^2 \frac{K_n K_m}{nm} \times\left[1-\exp\left(-n\frac{2\pi}{\lambda}d\right)\right] \times\left[1-\exp\left(-m\frac{2\pi}{\lambda}d\right)\right]\cos\left[(m-n)\frac{2\pi}{\lambda}x\right] \times\exp\left[-(m+n)\frac{2\pi}{\lambda}z\right]\right\}^{0.5}. \quad (34)$$

The Fourier components are given by (23).

V. Conclusion

MDS requires a magnetic field with a strong vertical gradient that changes with distance to the magnet but does not vary in the horizontal plane. Such a magnetic field can in principle only be generated by a pure harmonic sheet current with period λ. This period determines the decay rate of the exponentially decaying field magnitude. The obtainable separation resolution scales linearly with λ.

A practical magnet configuration that approximates this ideal current distribution consists of a planar array of racetrack coils with a characteristic leg width equal to one-third of the period λ.

Racetrack coils with a small thickness are inefficient, i.e., the usable magnetic field gradient at the fluid bed relative to the peak magnetic field in the coils is low. This can be explained by considering the Fourier components of the magnetic field. Also, the higher order Fourier components represent an unwanted ripple in the magnetic field profile. Their effect at the fluid bed is stronger for thin coils than for thick coils.

A further refinement of the current distribution can be achieved by a "notched" current profile, which reduces field ripples close to the magnet. This refinement also reduces the peak field in the conductor compared to simple racetracks. This effect is larger for thin winding packs. The downside is the added winding complexity. For the NbTi demonstrator magnet under construction at the University of Twente, it was decided to use three racetrack coils with a simple rectangular cross section.

The considerations in this work are applicable not just to MDS. They are valid for applications in general where a magnetic field gradient perpendicular to the magnet surface is required that changes with distance from the magnet and is constant in the parallel plane.

For an analysis of the optimum number of coils for a practical MDS system and the effects of using a system with finite dimensions, the reader is referred to [32], where the analytical results of this article are taken as a starting point for numerical calculations.

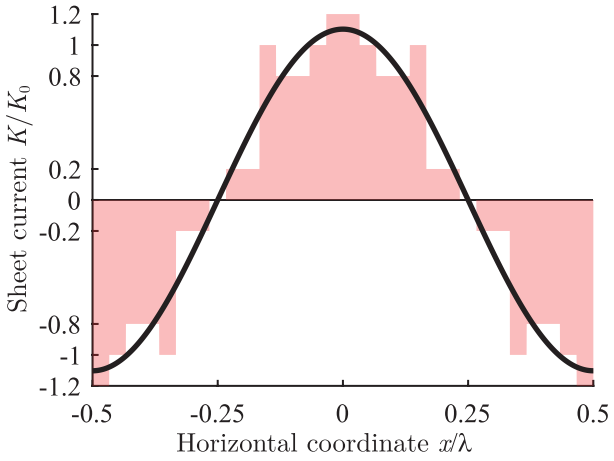

Fig. 13. Notched ($n = 5$ notches) current distribution with periodicity λ. The black line indicates the ideal harmonic current distribution.

Appendix
Further Approximation of Ideal Current Distribution

Here, a current distribution is considered that, compared to the rectangular racetrack coils, still more closely resembles the ideal current distribution. By adding five subdivisions of period $\lambda/5$ to the original rectangular current sheet profile, the current profile shown in Fig. 13 is obtained. In practice, this profile can be realized, e.g., by shaping the winding pack cross section, leaving out turns for certain x-values and adding turns elsewhere, so-called "notching." The effect of this notching is that it removes the K_5 component completely. Looking again at the magnitudes of the Fourier components (see Fig. 8), it can be seen that the largest remaining coefficient after K_1 is now K_7 and it has a magnitude of $K_1/7$ at $z = 0$.

One could in principle divide the winding pack into even smaller segments, thereby eliminating the higher order Fourier components. However, since the higher harmonics decay more quickly with the height z, the gain from eliminating these harmonics becomes smaller and is likely not worth the additional effort and added complexity. It will depend on the desired λ whether the improvements made are worth this effort, as for smaller periodicities, the near-coil region may be effectively enclosed in the cryostat.

For our NbTi demonstrator magnet, we decided to use racetrack coils with a simple rectangular cross section, as simplicity is valued above optimization for this first-of-a-kind magnet.

Acknowledgment

This work was supported in part by the Dutch Ministry of Economic Affairs. This research is part of the program Innovative Magnetic Density Separation (IMDS), which is supported by NWO, The Netherlands Organisation for Scientific Research, Domain Applied and Engineering Sciences.

References

[1] B. Hu, "Magnetic density separation of polyolefin wastes," Ph.D. dissertation, Dept. Civil Eng. Geosci., Univ. Delft, Delft, The Netherlands, 2014.

[2] E. J. Bakker, P. C. Rem, and N. Fraunholcz, "Upgrading mixed polyolefin waste with magnetic density separation," *Waste Manage.*, vol. 29, no. 5, pp. 1712–1717, May 2009.

[3] S. Serranti, V. Luciani, G. Bonifazi, B. Hu, and P. C. Rem, "An innovative recycling process to obtain pure polyethylene and polypropylene from household waste," *Waste Manage.*, vol. 35, pp. 12–20, Jan. 2015.

[4] L. Muchova, E. Bakker, and P. Rem, "Precious metals in municipal solid waste incineration bottom ash," *Water, Air, Soil Pollut., Focus*, vol. 9, nos. 1–2, pp. 107–116, Apr. 2009.

[5] E. J. Bakker, P. Rem, A. J. Berkhout, and L. Hartmann, "Turning magnetic density separation into green business using the cyclic innovation model," *Open Waste Manage. J.*, vol. 3, no. 1, pp. 99–116, Dec. 2010.

[6] V. Luciani, G. Bonifazi, P. Rem, and S. Serranti, "Upgrading of PVC rich wastes by magnetic density separation and hyperspectral imaging quality control," *Waste Manage.*, vol. 45, pp. 118–125, Nov. 2015.

[7] J. Oberteuffer, "Magnetic separation: A review of principles, devices, and applications," *IEEE Trans. Magn.*, vol. MAG-10, no. 2, pp. 223–238, Jun. 1974.

[8] J. Svoboda, *Magnetic Techniques for the Treatment of Materials*. Norwell, MA, USA: Kluwer, 2004.

[9] F. Luborsky and B. Drummond, "High gradient magnetic separation: Theory versus experiment," *IEEE Trans. Magn.*, vol. MAG-11, no. 6, pp. 1696–1700, Nov. 1975.

[10] M. Takayasu, R. Gerber, and F. Friedlaender, "Magnetic separation of submicron particles," *IEEE Trans. Magn.*, vol. MAG-19, no. 5, pp. 2112–2114, Sep. 1983.

[11] S. Trindade and H. Kolm, "Magnetic desulfurization of coal," *IEEE Trans. Magn.*, vol. MAG-9, no. 3, pp. 310–313, Sep. 1973.

[12] R. Oder, "High gradient magnetic separation theory and applications," *IEEE Trans. Magn.*, vol. MAG-12, no. 5, pp. 428–435, Sep. 1976.

[13] E. Hise, A. Holman, and F. Friedlaender, "Development of high-gradient and open-gradient magnet separation of dry fine coal," *IEEE Trans. Magn.*, vol. MAG-17, no. 6, pp. 3314–3316, Nov. 1981.

[14] D. Kelland, "High gradient magnetic separation applied to mineral beneficiation," *IEEE Trans. Magn.*, vol. MAG-9, no. 3, pp. 307–310, Sep. 1973.

[15] A. Nakahira, T. Kubo, and H. Murase, "Synthesis of LDH-type clay substituted with Fe and Ni ion for arsenic removal and its application to magnetic separation," *IEEE Trans. Magn.*, vol. 43, no. 6, pp. 2442–2444, May 2007.

[16] X. Zheng, Y. Wang, and D. Lu, "Effect of matrix shape on the capture of fine weakly magnetic minerals in high-gradient magnetic separation," *IEEE Trans. Magn.*, vol. 52, no. 9, pp. 1–11, Sep. 2016.

[17] J. Oberteuffer, I. Wechsler, P. Marston, and M. McNallan, "High gradient magnetic filtration of steel mill process and waste waters," *IEEE Trans. Magn.*, vol. MAG-11, no. 5, pp. 1591–1593, Sep. 1975.

[18] A. Pasteur, N. Tippkotter, P. Kampeis, and R. Ulber, "Optimization of high gradient magnetic separation filter units for the purification of fermentation products," *IEEE Trans. Magn.*, vol. 50, no. 10, pp. 1–7, Oct. 2014.

[19] L. Zhou, W. Li, Y. Han, Y. Li, and D. Liu, "Numerical simulation for magnetic field analysis and magnetic adsorption behavior of ellipse magnetic matrices in HGMS: Prediction magnetic adsorption behavior via numerical simulation," *Minerals Eng.*, vol. 167, Jun. 2021, Art. no. 106876.

[20] W. Ge, A. Encinas, E. Araujo, and S. Song, "Magnetic matrices used in high gradient magnetic separation (HGMS): A review," *Results Phys.*, vol. 7, pp. 4278–4286, Jan. 2017.

[21] D. Melville, F. Paul, and S. Roath, "High gradient magnetic separation of red cells from whole blood," *IEEE Trans. Magn.*, vol. MAG-11, no. 6, pp. 1701–1704, Nov. 1975.

[22] A. Hultgren, M. Tanase, C. S. Chen, and D. H. Reich, "High-yield cell separations using magnetic nanowires," *IEEE Trans. Magn.*, vol. 40, no. 4, pp. 2988–2990, Jul. 2004.

[23] K. Tsukada *et al.*, "Using magnetic field gradients to shorten the antigen-antibody reaction time for a magnetic immunoassay," *IEEE Trans. Magn.*, vol. 55, no. 7, pp. 1–5, Jul. 2019.

[24] D. Fletcher, R. Gerber, P. Lawson, and J. Boehm, "Eddy-current separation of non-ferrous conductors and non-conductors: Theory and initial experiments," *IEEE Trans. Magn.*, vol. 27, no. 6, pp. 5375–5377, Nov. 1991.

[25] J. Cui and E. Forssberg, "Mechanical recycling of waste electric and electronic equipment: A review," *J. Hazardous Mater.*, vol. 99, no. 3, pp. 243–263, May 2003.

[26] R. Kaiser and G. Miskolczy, "Some applications of ferrofluid magnetic colloids," *IEEE Trans. Magn.*, vol. MAG-6, no. 3, pp. 694–698, Sep. 1970.

[27] A. M. van Silfhout, H. Engelkamp, and B. H. Erné, "Colloidal stability of aqueous ferrofluids at 10 T," *J. Phys. Chem. Lett.*, vol. 11, no. 15, pp. 5908–5912, Aug. 2020.

[28] D. Fletcher, R. Gerber, and T. Moore, "An extended study of the electromagnetic separation of non-ferrous metals from insulators," *IEEE Trans. Magn.*, vol. 31, no. 6, pp. 4187–4189, Nov. 1995.

[29] K. Halbach, "Design of permanent multipole magnets with oriented rare earth cobalt material," *Nucl. Instrum. Methods*, vol. 169, no. 1, pp. 1–10, Feb. 1980.

[30] J. Mallinson, "One-sided fluxes—A magnetic curiosity?" *IEEE Trans. Magn.*, vol. MAG-9, no. 4, pp. 678–682, Dec. 1973.

[31] J. J. Kosse, M. Dhallé, G. Tomás, H. J. M. ter Brake, and H. H. J. ten Kate, "Performance estimates of superconducting magnetic density separation," to be published.

[32] J. J. Kosse, M. Dhallé, G. Tomás, P. C. Rem, H. J. M. ter Brake, and H. H. J. ten Kate, "Optimum coil-system layout for magnet-driven superconducting magnetic density separation," to be published.

[33] J. X. Jin *et al.*, "A high gradient magnetic separator fabricated using Bi-2223/Ag HTS tapes," *IEEE Trans. Appl. Supercond.*, vol. 9, no. 2, pp. 394–397, Jun. 1999.

[34] R. Gerber and M. Watmough, "A design of a superconducting split-coil open gradient magnetic separator," *IEEE Trans. Magn.*, vol. MAG-21, no. 5, pp. 2053–2055, Sep. 1985.

[35] J. Iannicelli *et al.*, "Magnetic separation of kaolin clay using a high temperature superconducting magnet system," *IEEE Trans. Appl. Supercond.*, vol. 7, no. 2, pp. 1061–1064, Jun. 1997.

[36] J. Boehm, R. Gerber, D. Fletcher, and M. R. Parker, "Deflection of weakly magnetic materials by superconducting OGMS," *IEEE Trans. Magn.*, vol. MAG-24, no. 2, pp. 1674–1676, Mar. 1988.

[37] D. D. Jackson, "Processing of China clays using a commercial-scale, conduction-cooled superconducting magnetic separation system," *IEEE Trans. Magn.*, vol. 49, no. 7, pp. 3438–3440, Jul. 2013.

[38] K. J. Binns, *The Analytical and Numerical Solution of Electric and Magnetic Fields*, Hoboken, NJ, USA: Wiley, 1992.

[39] H. Gobel, *Inventarisatie Scheidingstechnieken Harde Polyolefinen in Polypropyleen (PP) en Polyethyleen (PE)*. Mechelen, Belgium: The Public Waste Agency of Flanders (OVAM), 2009.

[40] V. Zermeño and F. Grilli, "3D modelling and simulation of 2G HTS stacks and coils," *Supercond. Sci. Technol.*, vol. 27, Mar. 2014, Art. no. 044025.

[41] Y. Iwasa, *Case Studies in Superconducting Magnets*. New York, NY, USA: Springer, 2009.

[42] M. N. Wilson, *Superconducting Magnets*. Oxford, U.K.: Clarendon, 1987.